Cosmological and astrophysical parameters from the Sloan Digital Sky Survey flux power spectrum and hydrodynamical simulations of the Lyman α forest

Matteo Viel[★] and Martin G. Haehnelt

Institute of Astronomy, Madingley Road, Cambridge CB3 0HA

ABSTRACT

The flux power spectrum of the Lyman α forest in quasar [quasi-stellar object (QSO)] absorption spectra is sensitive to a wide range of cosmological and astrophysical parameters and instrumental effects. Modelling the flux power spectrum in this large parameter space to an accuracy comparable to the statistical uncertainty of large samples of QSO spectra is very challenging. We use here a coarse grid of hydrodynamical simulations run with GADGET-2 to obtain a 'best-guess' model around which we calculate a finer grid of flux power spectra using a Taylor expansion of the flux power spectrum to first order. In this way, we investigate how the interplay between astrophysical and cosmological parameters affects their measurements using the recently published flux power spectrum obtained from 3035 Sloan Digital Sky Survey (SDSS) QSOs. We find that the SDSS flux power spectrum alone is able to constrain a wide range of parameters including the amplitude of the matter power spectrum σ_8, the matter density Ω_m, the spectral index of primordial density fluctuations n, the effective optical depth τ_{eff} and its evolution. The thermal history of the intergalactic medium (IGM) is, however, poorly constrained and the SDSS data favour either an unplausibly large temperature or an unplausibly steep temperature–density relation. By enforcing a thermal history of the IGM consistent with that inferred from high-resolution QSO spectra, we find the following values for the best-fitting model (assuming a flat universe with a cosmological constant and zero neutrino mass): $\Omega_m = 0.28 \pm 0.03$, $n = 0.95 \pm 0.04$ and $\sigma_8 = 0.91 \pm 0.07$ (1σ error bars). The values for σ_8 and n are consistent with those obtained by McDonald et al. with different simulations for similar assumptions. We argue, however, that the major uncertainties in this measurement are still systematic rather than statistical.

Key words: intergalactic medium – quasars: absorption lines – cosmological parameters – large-scale structure of Universe.

1 INTRODUCTION

The last few years have seen the establishment of the Lyman α (Lyα) forest as one of the major observational tools to probe the matter power spectrum. Measurements of the matter power spectrum from the Lyα forest data extend to smaller scales and probe a complementary redshift range than those using the cosmic microwave background (CMB), galaxy surveys or weak gravitational lensing. The Lyα forest is thus ideally suited to constrain cosmological parameters which affect the power spectrum on small scales like the neutrino mass and the mass of dark matter (DM) particles or isocurvature perturbations (Seljak et al. 2005; Viel et al. 2005a; Beltran et al. 2005). In a combined analysis with CMB data the

Lyα forest results have also been pivotal in tightening constraints on the power-law index of the power spectrum of primordial density fluctuations n.

A consistent picture emerges suggesting that the fluctuation amplitude of the matter power spectrum σ_8 is rather high, that the spectral index of primordial density fluctuations is consistent with the value $n = 1$ and that there is no evidence for a running of the spectral index, significant neutrino mass or a deviation from a cold dark matter (CDM) spectrum at small scales. (Croft et al. 1998, 2002 [C02]; McDonald et al. 2000, 2004 [M04a], 2004b [M04b]; Hui et al. 2001; McDonald 2003, Desjacques et al. 2004; Viel et al. 2003, 2005; Viel, Haehnelt & Springel 2004b [VHS], Viel, Weller & Haehnelt 2004c; Lidz et al. 2005). Major uncertainties are thereby the assumed effective optical depth and thermal history of the intergalactic medium (IGM) and the numerical limitations in obtaining accurate theoretical

[★]E-mail: viel@ast.cam.ac.uk

predictions for the flux power spectrum for a large parameter space (see VHS and M04a for a detailed discussion).

VHS and Viel et al. (2004c) recovered the linear DM power spectrum amplitude and its slope from a new set of 27 high-resolution high signal-to-noise ratio (S/N) quasi-stellar objects (QSOs; the Large UVES Quasar Absorption Spectra, or LUQAS, sample, Kim et al. 2004 [K04]) and re-analysed the earlier results of C02. Viel et al. (2004c) found $\sigma_8 = 0.94 \pm 0.08$ and $n = 0.99 \pm 0.03$ (1σ) and no evidence for a (large) running spectral index when they combined the Lyα forest data with the *Wilkinson Microwave Anisotropy Probe* (*WMAP*) data. Similar results have been obtained subsequently by the Sloan Digital Sky Survey (SDSS) collaboration from a much larger sample of 3035 low-resolution low-S/N spectra with significantly wider redshift coverage (M04b; Seljak et al. 2005). These findings corrected earlier claims of Spergel et al. (2003) who used the data of C02 combined with cosmic microwave background (CMB) and galaxy survey data to argue for a significant tilt away from the canonical Harrison–Zeldovich $n = 1$ spectrum and possibly also for a running of the spectral index [see Seljak, McDonald & Makarov (2003) for the first suggestion that this result may be due to the assumption of an unplausibly large effective optical depth].

Large samples of QSO absorption spectra offer the opportunity to obtain the flux power spectrum for a wide range of redshifts with an accuracy at the per cent level. Despite the generally good agreement between different groups achieved in the last couple of years there are, however, still major open issues of what and how large the uncertainties in the cosmological and astrophysical parameters inferred from the flux power spectrum are (see VHS and M04b for discussions with different views). It will be important to resolve these issues if further progress is to be made.

The two data sets used by VHS and M04b and their theoretical modelling were very different. The SDSS QSO data set analysed by M04a consists of 3035 QSO spectra at low resolution ($R \sim 2000$) and low S/N (~ 10 per pixel) spanning a wide range of redshifts, while the LUQAS and the C02 samples contain mainly high-resolution ($R \sim 45000$), high-S/N (>50 per pixel) QSO spectra with median redshifts of $z = 2.125$ and 2.725, respectively. The analysis methods to infer cosmological and astrophysical parameters were also very different. M04b modelled the flux power spectrum using a large number of Hydro Particle Mesh (HPM) simulations (Gnedin & Hui 1998; Viel, Haehnelt & Springel 2005b) exploring a large multidimensional parameter space. Viel et al. (2004b) improved instead the effective bias method developed by C02. They used a grid of full hydrodynamical simulations run with the Tree-smoothed particle hydrodynamics (SPH) code GADGET-2 (Springel, Yoshida & White 2001; Springel 2005) to invert the non-linear relation between flux and matter power spectrum.

Both methods have their own set of problems. M04b had to use the approximate HPM method which they could only calibrate on a small number of hydrodynamical simulations of small box size [see Viel et al. (2005b) for a discussion of the accuracy of HPM simulations]. M04b further had to compromise on box size and even time-stepping in order to explore a large parameter space. This leads to large number of uncertain corrections which added to another large set of corrections necessary because of the rather low resolution and S/N of their data. The method used by VHS on the other hand requires differentiating the 1D flux power spectrum to obtain the '3D' flux power spectrum, which introduces rather large errors. This makes the assessment of statistical errors somewhat difficult. We refer to Zaldarriaga et al. (2001), Gnedin & Hamilton (2002), Zaldarriaga et al. (2003) and Seljak et al. (2003) for a further critical assessment of the use of the effective bias method to infer cosmological parameters. VHS concluded that the best they can do was to give an estimate of the many systematic uncertainties involved and to combine these in a conservative way in the final result. However, for attempts to take advantage of the full redshift coverage and smaller errors of the observed SDDS flux power spectrum the effective bias stops being useful.

Further motivated by the differences in the data and in the theoretical modelling performed by the two groups, we will analyse here the SDSS flux power spectrum with high-resolution, large box-size full hydrodynamical simulations. Ideally, one would like to be able to repeat the analysis made by the SDSS collaboration by using a very fine grid of full hydrodynamical simulations in order to be able to sample the multidimensional parameter space. However, at present, this approach is not feasible since hydrodynamical simulations are very time consuming. We therefore decided to concentrate most of the analysis on a small region of the parameter space, around the best-fitting models obtained by the two groups. We thereby use a Taylor expansion to approximate the flux power spectrum around a best-guess model. This approximation should be reasonably accurate for little displacements in parameter space. We have checked the validity of the approximation for a few models. However, we caution the reader that the final error bars on recovered astrophysical and cosmological parameters are likely to be somewhat underestimated due to unaccounted errors of this approximation.

The plan of this paper is as follows. In Section 2, we briefly describe the SDSS data set, while the hydrodynamical simulations are discussed in Section 3. Section 4 describes the technical details of our modelling of the flux power spectrum and the reader more interested in the results may go straight to Section 5 where we discuss our findings for the cosmological and astrophysical parameters. Section 6 contains a summary and an outline of possible ways of improving these measurements.

2 THE SLOAN DIGITAL SKY SURVEY FLUX POWER SPECTRUM

McDonald et al. (2004a) have presented the flux power spectrum of a large sample of 3035 absorption spectra of QSO in the redshift range $2 < z < 4$ drawn from the DR1 and DR2 data releases of SDSS. With a spectral resolution of $R \sim 2000$ the typical absorption features with a width of ~ 30 km s^{-1} are not resolved. The S/N of the individual spectra is rather low, S/N ~ 10 per pixel. The large number of spectra means, however, that the flux power spectrum on scales a factor of a few larger than the thermal cut-off can be measured with small statistical errors. M04a have re-analysed the raw absorption spectra and have investigated the effect of noise, resolution of the spectrograph, sky subtraction, quasar continuum and associated metal absorption. M04a make corrections for these effects and give estimates of the errors for the most important of these corrections. The corrections are not small. The noise contribution to the flux power spectrum rises from 15–30 per cent at the smallest wavenumbers to order of unity at the largest wavenumbers and varies with redshift. The corrections for uncorrelated metal absorption are generally a factor of 5–10 smaller than this. The correction for resolution varies from 1 per cent at the smallest wavenumbers to a factor of 4 at the largest wavenumbers. M04a also identified a correlated Si III feature in the absorption spectra for which they present an empirical fit to the effect on the flux power spectrum. As a final result of their analysis M04a present their best estimate for the flux power spectrum $P_F(k, z)$ at 12 wavenumbers in the range $0.00141 < k < 0.01778$ s km^{-1}, equally spaced in $\Delta \log k = 0.1$ for $z = 2.2, 2.4, 2.6, 2.8, 3, 3.2, 3.4, 3.6, 3.8, 4$ and 4.2. At the time

we started this work the two highest-redshift bins were not publicly available so we will not use them in the following analysis. We will here use this flux power spectrum together with the recommended corrections to the data and the recommended treatment of the errors of these corrections. We will come back to this in more detail in Section 4.2.1 Note that we have also dropped the highest-redshift bin at $z = 3.8$ as we could not fit it well with our models for the flux power spectrum (see Section 4.3 for more details).

3 HYDRODYNAMICAL SIMULATIONS

We have run a suite of full hydrodynamical simulations with GADGET-2 (Springel et al. 2001; Springel 2005) similar to those in VHS. We have varied the cosmological parameters, particle number, resolution, box size and thermal history of the simulations. In Table 1 we list the fluctuation amplitude σ_8, the spectral index n as well as box size and number of particles of the different simulations (note that few of these simulations are actually the same as those presented in VHS). The box size and particle number are given in a form such that 60–400 corresponds to a box of length $60\,h^{-1}$ Mpc with 2×400^3 (gas + DM) particles. Note that this is the box size of the simulations used for our final analysis and is a factor of 6 larger than the largest of the hydrodynamical simulations used by M04b.

GADGET-2 was used in its TreePM mode and we have used a simplified star formation criterion which speeds up the calculations considerably. The simulations were performed with periodic boundary conditions with an equal number of DM and gas particles and used the conservative 'entropy formulation' of SPH proposed by Springel & Hernquist (2002). The cosmological parameters are close to the values obtained by the *WMAP* team in their combined analysis of CMB and other data (Spergel et al. 2003). All but two of the simulations in Table 1 have the following parameters: $\Omega_m = 0.26$, Ω_Λ

Table 1. Grid of hydrodynamical cosmological simulations.

Simulation	σ_8	n	box $- N_p^{1/3}$	χ^2_{min} [a]
B1	0.7	0.95	60–400	124.1
B1.5	0.775	0.95	60–400	113.2
B2	0.85	0.95	60–400	104.7
B2.5	0.925	0.95	60–400	101.2
B3	1	0.95	60–400	107.7
B3.5	1.075	0.95	60–400	132.8
C2	0.85	1	60–400	127.8
C3	1	1	60–400	121.2
B2$_{30\,200}$	0.85	0.95	30–200	–
B2$_{H_0}$ [b]	0.85	0.95	30–200	–
B2$_{\Omega_m}$ [c]	0.85	0.95	30–200	–
B2$_{ne}$ [d]	0.85	0.95	30–200	–
B2$_{nec}$ [e]	0.85	0.95	30–200	–
B2$_{lf}$ [f]	0.85	0.95	30–200	–
B2$_{hr}$ [g]	0.85	0.95	30–200	–
B2$_{cold}$ [h]	0.85	0.95	30–200	–
B2$_{30\,400}$	0.85	0.95	30–400	–
B2$_{120\,400}$	0.85	0.95	120–400	–

[a] χ^2_{min} is for 88 d.o.f. (96 data points, eight free parameters for the effective optical depth at the eight different redshifts) errors for the noise and resolution corrections are treated as suggested in M04a. [b] $H_0 = 80$ km s^{-1} Mpc^{-1}. [c] $\Omega_m = 0.30$. [d] Simulation with non-equilibrium solver with re-ionization at $z \sim 6$. [e] Non-equation colder version with re-ionization at $z \sim 6$. [f] Non-equation version with late re-ionization at $z \sim 4$. [g] Non-equation version with early re-ionization at $z \sim 17$. [h] Same as $B2_{30\,200}$ (equilibrium with re-ionization at $z \sim 6$) but with colder equation of state to match the evolution of B2$_{hr}$ at $z < 4$.

$= 0.74$, $\Omega_b = 0.0463$ and $H_0 = 72$ km s^{-1} Mpc^{-1}. The CDM transfer functions of all models have been taken from Eisenstein & Hu (1999). For the remaining two simulations the Hubble constant and matter density were varied to $\Omega_m = 0.3$ and $H_0 = 80$ km s^{-1} Mpc^{-1}, respectively. To facilitate a comparison with M04b we also give the amplitude of the linear power spectrum at the pivot wavenumber k_p used by M04b, $\Delta_L^2 (k_p = 0.009\,\text{s km}^{-1}, z_p = 3) = 0.350$ and the effective spectral index $n_{eff} = \text{d} \ln P_L / \text{d} \ln k = -2.33$ for the B2 simulation.

Most of the simulations were run with the *equilibrium* solver for the evolution of the ionization balance and temperature implemented in the public version of GADGET-2 (which assumes the gas to be in photoionization equilibrium) with a ultraviolet (UV) background produced by quasars as given by Haardt & Madau (1996), which leads to re-ionization of the Universe at $z \simeq 6$. The assumption of photoionization equilibrium is valid for most of the evolution of the IGM responsible for the Lyα forest. It is, however, a bad approximation during re-ionization, where it leads to an underestimate of the photoheating rate and as a result to too low temperatures and generally too steep a temperature–density relation (Theuns et al. 1998). For the models run with the equilibrium solver we have thus as before increased the heating rates by a factor of 3.3 at $z > 3.2$ in order to take into account the underestimate of the photoheating due to the equilibrium solver and optical-depth effects for the photoheating of helium before helium is fully re-ionized at ~ 3.2 (Abel & Haehnelt 1999). This is necessary to obtain temperatures close to observed temperatures (Ricotti, Gnedin & Shull 2000; Schaye et al. 2000).

Some simulations were run with a *non-equilibrium* solver which has been implemented by James Bolton into GADGET-2. For the simulations run with the non-equilibrium solver only the optical-depth effects for the photoheating of helium have to be taken into account. The increase of the photoheating rates at $z > 2$ necessary to match observed temperatures was thus only a factor of 1.8. We have varied the thermal history of the simulations by re-mapping the redshift evolution of the UV background. For more details on the simulations and the non-equilibrium solver we refer to VHS, Bolton et al. (2005a,b) and Section 4.2.3.

4 MODELLING THE SLOAN DIGITAL SKY SURVEY FLUX POWER SPECTRUM USING HYDRODYNAMICAL SIMULATIONS

4.1 A two-step approach

Hydrodynamical simulations are rather expensive in terms of central processing unit (CPU) time. A typical simulation used in the analysis of VHS took two weeks of wall-clock time to reach $z = 2$ on 32 processors on COSMOS, an SGI Altix 3700. This made it impossible to fully sample a large multidimensional parameter space with full hydrodynamical simulations. With the rather modest numerical resources available to us we have thus decided to take the following approach.

We have first run a range of simulations with cosmological parameters close to those inferred by VHS and M04b which allowed us to explore a wider range of thermal histories of the IGM to better understand the resulting uncertainties. We have then fitted the simulated flux power spectra to the SDSS flux power spectrum as described in Section 5. Based on this and our previous studies in VHS we have chosen a 'best-guess' model which fits the data well. To improve our parameter choices further and to get at least approximate error estimates we have then explored a large multidimensional parameter

space around our best-guess model. This also enabled us to explore the degeneracies between different parameters. In order to keep the required CPU time at a manageable level we have approximated the flux power spectra by a Taylor expansion to first order around our best-guess model. If p is an arbitrary parameter vector close to the best-guess model described by p_0, we have assumed that:

$$P_{\mathrm{F}}(k, z; p) = P_{\mathrm{F}}(k, z; p^0) +$$
$$+ \sum_{i}^{N} \frac{\partial P_{\mathrm{F}}(k, z; p_i)}{\partial p_i}\bigg|_{p=p^0} (p_i - p_i^0), \qquad (1)$$

where p_i are the N components of the vector p. This requires the determination of only N derivatives which can be estimated by running one simulation each close to the best-guess model. Obviously, this linear approximation will only hold as long as the changes in the flux power spectrum are small. Within 1–2σ of the best-guess model this should, however, be the case. We have explicitly checked how these derivatives change around another fiducial model for some of the parameters and we will quantify this in Section 4.4. Once the derivatives are obtained we can then calculate an arbitrarily fine grid of flux power spectra around the best-guess model with equation (1).

4.2 Systematic uncertainties

As discussed in detail by VHS and M04b there is a wide range of systematic uncertainties in the analysis of the flux power spectrum. The origins of these uncertainties fall broadly into the following five categories.

(i) Deficiencies of the data which have to be corrected;

(ii) uncertainty of the effective optical depth;

(iii) uncertainty of the thermal state of the IGM;

(iv) lack of ability to make accurate predictions of the flux power spectrum for a large parameter space; and

(v) lack of ability to model other physical processes which potentially affect the flux power spectrum.

We will discuss the resulting systematic uncertainties in turn.

4.2.1 Correction to the data

M04b have applied a number of corrections for noise, resolution and the correlated Si III feature identified by M04a. We have adopted the same corrections which are summarized below. For more details we refer to M04a and M04b. We allow for an error in the k-dependent noise correction at each redshift by subtracting $f_i P_{\text{noise}}(k, z_i)$ from $P_{\mathrm{F}}(k, z)$ and treat the f_i as free parameter in the fit. M04b recommend to assume that the distribution of f_i is Gaussian with mean zero and width 0.05 which corresponds to a typical error in the noise correction of 5 per cent. M04a further recommend to allow for an overall error on the resolution correction, by multiplying $P_{\mathrm{F}}(k, z)$ with $\exp(\alpha k^2)$, where α is treated as a free parameter with Gaussian distribution with mean zero and width $(7\,\mathrm{km\,s^{-1}})^2$. To account for contamination by the correlated Si III feature we modify our model flux power spectra as suggested as follows: $P_{\mathrm{F}}(k) = (1 + a^2) P_{\text{sim}}(k) + 2a \cos(v k) P_{\text{sim}}(k)$ with $a = f_{\text{Si III}}/[1 - \overline{F}(z)]$, $f_{\text{Si III}} = 0.11$ and $v = 2271\,\mathrm{km\,s^{-1}}$. The noise and resolution corrections and their errors depend strongly on the wavenumber k as shown in Fig. 1. Note that M04a also subtracted a contribution of uncorrelated associated metal absorption which they estimated redward of the Lyα emission line. The effect of continuum-fitting errors on the flux power spectrum is a further uncertainty which is discussed in K04, M04a and Tytler et al. (2004). Continuum-fitting errors are difficult to quantify and we again follow M04b in not attempting to model them.
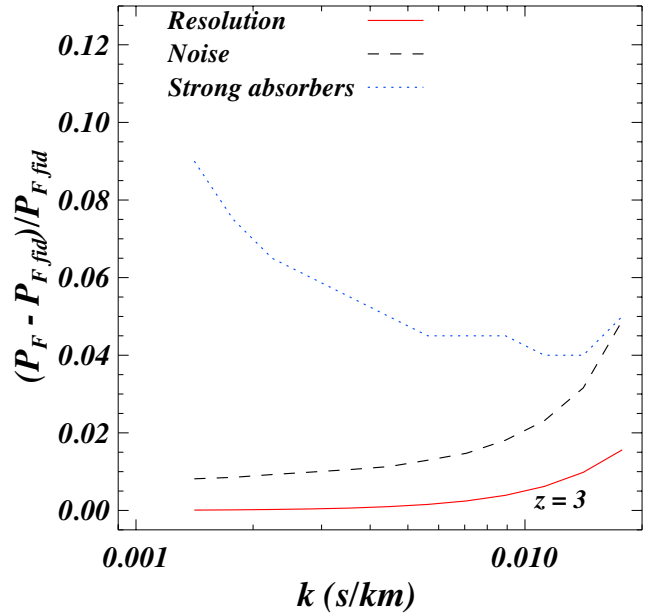

Figure 1. The dashed, solid and dotted curves show the effect of the error in the noise correction and resolution and the correction for strong absorption systems, respectively. We show fractional differences in the flux power spectrum at $z = 3$. Note that we assume only the error of the noise correction to depend on redshift. The changes correspond to an error of 5 per cent in the noise correction and of $(7\,\mathrm{km\,s^{-1}})^2$ in the resolution (see Section 4.2.1 for more details).

4.2.2 Uncertainty of the effective optical depth

As discussed in VHS and Seljak et al. (2003) the poorly known effective optical depth results in major uncertainties in any analysis of the Lyα forest flux power spectrum. The effective optical depth is to a large extent degenerate with the amplitude of the matter power spectrum. As shown in M04b the k dependence of changes in the flux power spectrum due to varying effective optical depth and amplitude of the matter power spectrum is, however, somewhat different. This allows – at least in principle – to break this degeneracy. We will come back to this point later. When modelling the effective optical depth we will investigate two cases. We will either let the effective optical depth vary independently in the different redshift bins or we will parametrize the evolution of the effective optical depth as a power law in redshift.

4.2.3 Uncertainties due to the thermal state of the IGM

In order to explore in more detail the uncertainties due to thermal effects on the flux power spectrum we have run simulations with a wide range of thermal histories (Table 1). Note that this is different from VHS where we have only performed a posteriori re-scalings of the temperature–density relation to investigate thermal effects. We have calculated the value T_0 as the median temperature of gas with logarithmic overdensity values between -0.1 and 0.1. The value of γ we determined from the slope of the temperature–density relation for gas at mean density and 1.1 times the mean density.

In the left-hand panel of Fig. 2 we plot the different thermal histories (temperature at mean density in the bottom panel and γ in the top panel). The linestyles denote the different models as follows. The continuous curve is our standard B2 model with the equilibrium solver. The dashed curves show the same model with the non-equilibrium solver ($B2_{\text{ne}}$) which results in a significantly smaller
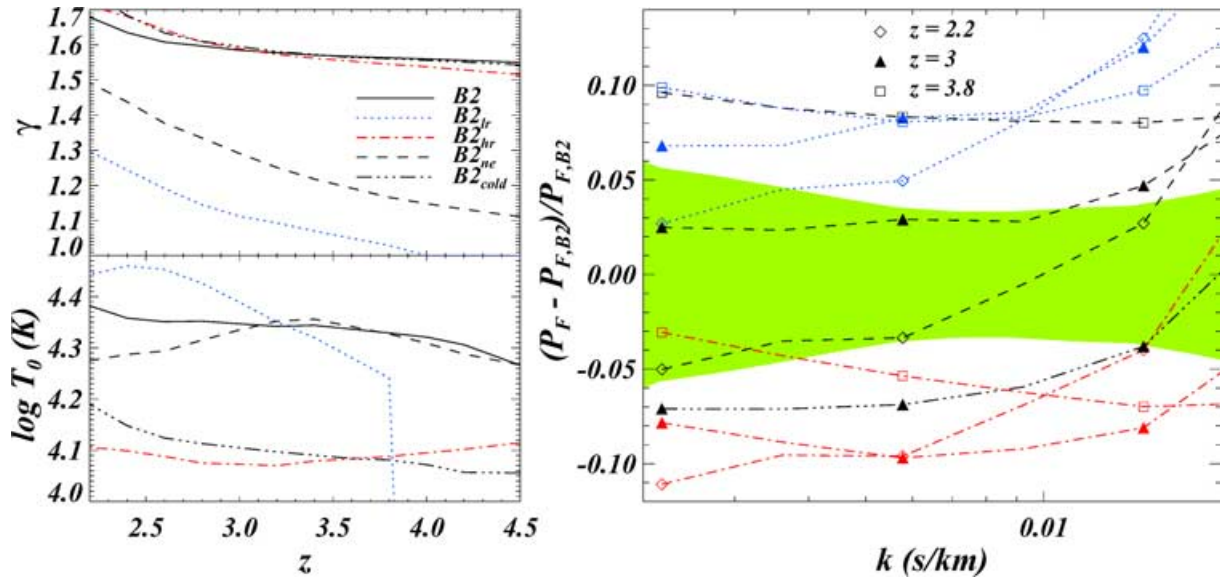
Figure 2. Left-hand (bottom panel): evolution of T_0 with redshift for different thermal histories: B2, the fiducial equilibrium model with re-ionization at $z \sim 6$ (continuous curve); B2$_{lr}$, simulation with a non-equilibrium solver with late re-ionization at $z \sim 4$ (dotted curve); B2$_{hr}$, non-equilibrium, with early re-ionization at $z \sim 17$ (dot–dashed curve); B2$_{ne}$, non-equilibrium with re-ionization at $z \sim 6$ (dashed curve); B2$_{cold}$, equilibrium with re-ionization at $z \sim 6$ and with a colder equation of state (triple dot–dashed curve). Left-hand (top panel): evolution of γ with redshift. Right-hand panel: fractional differences between the flux power spectrum of the different models compared to the fiducial model B2 at $z = 2.2$, 3 and 3.8 (diamonds, triangles and squares, respectively). For B2$_{cold}$ differences are only shown for $z = 3$, the other two redshifts are very similar. The shaded region indicates the statistical errors at $z = 3$.

γ. The dotted and dot–dashed curves show the same model with the non-equilibrium solver for late re-ionization at $z \sim 4$ ($B2_{lr}$) and early re-ionization at $z \sim 17$ ($B2_{hr}$). Finally, the triple dot–dashed curves show a model with re-ionization at $z \sim 6$ but smaller heating rate and thus a lower temperature, similar to that of $B2_{hr}$.

In the right-hand panel we show the differences of the flux power spectrum relative to our fiducial model $B2$ at three different redshifts. The differences are typically $\sim$5–10 per cent. Comparing $B2$ and $B2_{hr}$, which have a similar redshift evolution we find, for example, that a decrease of T_0 by 50 per cent ($\sim$10 000 K) results in a decrease in the flux power larger than 5 per cent. The effect of changing γ can be judged by comparing $B2_{ne}$ and $B2_{lr}$ at $z = 3$ which have approximately the same temperature. Decreasing γ by $\Delta \gamma = -0.5$ (-0.3) produces an increase in the flux power by 7.5 per cent (2.5 per cent), but we note that for $k > 0.01 \, \mathrm{s \, km}^{-1}$ the differences increase strongly.

We will later model the evolution of the thermal state of the IGM with redshift as broken power laws for temperature and slope of the temperature–density relation.

4.2.4 Uncertainties due to the modelling of the flux power spectrum

Modelling the flux power spectrum accurately is numerically challenging and checks for convergence are important. We have chosen to use here full hydrodynamical simulations performed with GADGET-2 described in Section 3. In VHS we found that simulations with a box size 60 h^{-1} Mpc and with 2×400^3 particles (60 400) are the best compromise for the analysis of the LUQAS sample. The lower-resolution SDSS power spectrum is not affected on large scale in the same way by continuum-fitting errors as the high-resolution spectra which we used in VHS and for which continuum-fitting errors appear to increase the flux power significantly at and above the scale corresponding to one Echelle order (Kim et al. 2004). The

usable range of wavenumbers is thus shifted to larger scales compared to flux power spectra obtained from high-resolution Echelle data. Ideally, one would thus like a somewhat larger box size than that used in VHS. Unfortunately, this is currently not feasible with simulations that at least marginally resolve the Jeans length. We have thus decided to use simulations with the same box size and resolution as in VHS.

Box size. For the final analysis we use simulations of 60 h^{-1} Mpc and with 2×400^3 particles (60 400). Since the error bars for the observed 1D flux power spectrum are significantly smaller than those of the 3D flux power spectrum used by VHS we checked whether or not the flux power spectrum is affected by box size and/or limited resolution at the per cent level. We have first checked how well the largest scales probed by SDSS are sampled by our fiducial (60 400) simulations. In VHS this was not an issue since the first data point used in the analysis was at $k = 0.003 \, \mathrm{s \, km}^{-1}$, which was well sampled by the (60 400) simulations. Our analysis here extends however to $k = 0.001 \, \mathrm{s \, km}^{-1}$ and could be affected by cosmic variance. To test this, we have compared the flux power spectrum of our fiducial (60 400) simulation B2 with that of a (120 400) simulation of the same model (B2$_{120\,400}$). The power of the latter at $k < 0.003 \, \mathrm{s \, km}^{-1}$ is typically larger by $\sim$3, 4 and 9 per cent at $z = 2.2$, 3 and 3.8, respectively. We correct for this by multiplying the flux power spectrum of the (60 400) simulation by corresponding factors. We will later use simulations with a factor of 2 smaller box size but the same resolution as our fiducial simulation to explore the effects of the thermal history. We have thus also compared the flux power spectrum of our fiducial (60 400) simulation B2 with a (30 200) simulation of the same model (B2$_{30\,200}$) and find that the latter underestimates the power by $\lesssim$3 per cent in the range $0.003 < k < 0.03 \, \mathrm{s \, km}^{-1}$ at $z = 2.2$, 3 and 4. Our findings regarding the dependence of the flux power spectrum on the thermal history of the IGM should thus be little affected by the fact that they were obtained from simulations of smaller box size.

Resolution. To quantify the effect of resolution, we compare the simulation B2$_{30\,200}$ with B2$_{30\,400}$ a simulation which has the same box size but eight times better mass resolution. The differences between B2$_{30\,400}$ and B2$_{30\,200}$ are less than 5 per cent for $k <$ 0.01 s km^{-1}, at any redshift, (3 per cent in the range $0.004 < k$ < 0.01 s km^{-1}. At $k = 0.02$ s km^{-1}, the flux power spectrum of B2$_{30\,400}$ is larger by $\sim$4 and 12 per cent at $z = 3$ and 4, respectively. This is in agreement with the findings of M04b. We will correct for the limited resolution by multiplying the flux power spectrum of our fiducial (60 400) simulation by corresponding factors. Both the resolution and box-size errors are comparable or smaller than the statistical errors of the flux power spectrum. We explicitly checked that these corrections do not significantly affect the parameters of our best-fitting model. They do, however, affect the $\chi^2_{\min}$ value of the best-fitting model. Note that both the resolution and box-size corrections could be model-dependent.

High-column density systems/damped Lyα systems. We have recently pointed out that the absorption profiles of high-column density systems/damped Lyα systems have a significant effect on the flux power spectrum over a wide range of scales (Viel et al. 2004a). These absorption systems are caused by high-redshift galaxies and the gas in their immediate vicinity. Numerical simulations still struggle to reproduce these systems correctly and they are thus a major factor of uncertainty in modelling the flux power spectrum. M04b have modelled the expected effect on the SDSS flux power spectrum and we have included this correction using the k dependence of Fig. 11 in M04b. M04b recommend to assume that the distribution of the correction made $A_{\rm damp}$ is Gaussian with mean 1 and width 0.3. The correction is shown in Fig. 1 as the dotted curve. It is of the order of 10 per cent at the largest scales and drops to 3 per cent at the smallest scales. Note that unlike M04b we have assumed that this correction does not vary with redshift.

4.2.5 *Uncertainties due to UV fluctuations, galactic winds, re-ionization history, temperature fluctuations*

There are a range of physical processes some of which are difficult to model, that are described below. Note that we have chosen not to try to include these effects in our analysis.

Spatial fluctuations of the H I ionization rate. The flux power spectrum is obviously sensitive to the neutral fraction of hydrogen which depends on the H I ionization rate. At low redshift $z <$ 3 the mean free path of ionizing photons is sufficiently large that spatial fluctuations of the H I rate should be too small to affect the flux power spectrum relevant for our investigation here (Croft 2004; Meiksin & White 2004; McDonald et al. 2005). At higher redshift this is less obvious. Quantitative modelling of the fluctuations requires, however, a detailed knowledge of the source distribution of ionizing photons which is currently not available. As we will discuss below there may be some tentative evidence that UV fluctuations do become important at the highest redshifts of the SDSS flux power spectrum sample.

Galactic winds. There is undeniable observational evidence that the Lyα forest has been affected by galactic winds. Associated metal absorption is found to rather low optical depth (Cowie et al. 1995; Schaye et al. 2003). Searches for the effect of galactic winds on QSO absorption spectra from Lyman break galaxies close to the line-of-sight have also been successful. The volume-filling factor of galactic winds and the material enriched with metals is, however, very uncertain (e.g. Pieri & Haehnelt 2004; Adelberger et al. 2005; Rauch et al. 2005). Numerical simulations have generally shown the effect of galactic winds to be small (Theuns et al. 2002a; Kollmeier

et al. 2003; Desjacques et al. 2004; Kollmeier et al. 2005; McDonald et al. 2005).

Temperature fluctuations. It is rather difficult to measure mean values of the temperature and little is known observationally about spatial fluctuations of the temperature (Theuns et al. 2002b). In the redshift range of interest the heating rate of the IGM should be dominated by photoheating of helium before helium is fully re-ionized. Helium re-ionization should thus lead to spatial temperature fluctuations (McDonald et al. 2000), which will affect the neutral fraction of hydrogen through the temperature dependence of the recombination coefficient. Temperature fluctuation may thus affect the flux power spectrum. Quantitative modelling of their effect on the flux power spectrum requires numerical simulation of helium re-ionization including full radiative transfer and good knowledge of the spatial distribution of the source of He II ionizing photons. Such modelling will also be uncertain.

Re-ionization history. The flux power spectrum is not only sensitive to the current thermal state of the IGM but also to its past thermal history. This is because the spatial distribution of the gas is affected by pressure effects (Hui & Gnedin 1997; Theuns, Schaye & Haehnelt 2000; Zaldarriaga, Hui & Tegmark 2001). Quantitative modelling of this effect is, however, again very uncertain as the heating rate at high redshift is expected to be dominated by photoheating of helium. In order to get a feeling for the effect of a simple change of the redshift when re-ionization occurs we can compare $B2_{\rm cold}$ and $B2_{\rm hr}$ at $z = 3$. Both simulations have approximately the same values for T_0 and γ at $z < 4$ while re-ionization occurs at $z \sim 6$ and $\sim$17, respectively. The differences are of the order of 3 per cent, in agreement with the findings of M04a.

4.3 Finding a 'best-guess' model

In order to settle on a best-guess model we have started with the coarse grid of hydrodynamical simulations presented in VHS. We have complemented this with simulations of a wider range of σ_8 and a wider range of thermal histories. We have fitted the flux power spectrum of all (60 400) simulations listed in Table 1 to the SDSS flux power spectrum allowing for errors in the correction to the data as described in Section 4.2.1 We thereby leave the effective optical depth as a free parameter at all redshifts.

The last column in Table 1 gives the resulting $\chi^2_{\min}$ values obtained using the full covariance matrix as given by M04a.[1] When performing the fits we noted that the highest-redshift bin at $z = 3.8$ is generally fitted very poorly. Omitting these 12 data points usually reduced the χ^2 by about 26 per cent for 11 degrees of freedom (d.o.f.). This may either indicate some problem with the data or some insufficiency of the model. The latter would require, however, a very rapid change of the model with redshift as dropping any of the other redshift bins reduced the χ^2 by the expected amount. UV fluctuations are probably the most plausible candidates for a rapid change towards the highest-redshift bin. We have decided to drop the highest-redshift bin for our analysis. This leaves 96 data points and eight free (unconstrained) parameters corresponding to 88 d.o.f.

The best-fitting simulation appears to be B2.5 which has $\chi^2_{\min} =$ 101.2, when minimizing over the noise array f_i, the resolution α and the effective optical depth. The simulation B2 has a $\chi^2_{\min} = 104.7$ close to that of B2.5, while the other models have typically $\Delta\chi^2 >$ 10. We regard these two models, with their thermal histories, as

---

[1] http://feynman.princeton.edu/~pmcdonal/LyaF/sdss.html.

reasonable good fits to the data set (χ^2 values higher than the quoted values have a probability of 16 and 11 per cent to occur).

We decided to choose B2 as our best-guess model despite the fact B2 has a somewhat larger χ^2 value than B2.5 for two reasons. First, the model is surprisingly close to the best-fitting model quoted by M04a (which has $\Omega_m = 0.3$, $\sigma_8 = 0.85$, $n = 0.94$ and $h = 0.7$). Secondly, we had already run more simulations exploring different thermal histories for B2 than for the other models. We have, however, checked as discussed in more detail in Section 5 that an expansion around the B2.5 model gives essentially the same results in terms of the inferred astrophysical and cosmological parameters.

4.4 Derivatives of the flux power spectrum of the 'best-guess' model

The key ingredients for our estimates of a fine grid of flux power spectra are the derivatives of the flux power spectrum (see equation 1) close to the best-guess model B2. Fig. 3 shows the k dependence of the most relevant of these derivatives at three redshifts ($z = 2.2, 3$ and 3.8 from left-hand side to right-hand side) in the form of the change of the flux power spectrum for a finite change of the parameters. We compute these derivatives at the wavenumbers of the SDSS flux power spectrum, although we cannot directly cover the two smallest wavenumbers because we are using (30 200) simulations to estimate these derivatives. For these two points we have used an extrapolation with a second-order polynomial. This should be a reasonable approximation given the rather weak and smooth k dependence at these scales.

In the top panel we show how the flux power spectrum depends on σ_8, n, τ_{eff}. A 5 per cent increase in the effective optical depth, translates into a 7 per cent increase in the flux power spectrum with no dependence on redshift and with very little (<1 per cent) dependence on wavenumber. A change of the spectral index by $\Delta n = 0.05$ leads to an increase of the flux power which rises steeply with wavenumber from 1 to 4–6 per cent, while increasing σ_8 by 9 per cent increases the flux power by 5–6 per cent for $k < 0.01 \, (\mathrm{s \, km^{-1}})$ dropping to ~ 2 per cent at the smallest scales considered here. The changes introduced by different values of Ω_m and H_0 are shown in the middle panel. An increase of the Hubble parameter by 8 km s^{-1} Mpc^{-1} leads to an increase of the order of 3 per cent, while the change due to an increase of Ω_m shows a peak at $k \sim 0.01$ s km^{-1} of 3 per cent at $z = 3.8$ and depends less strongly on wavenumber at lower redshifts. The derivatives of the flux power spectrum with respect to changes in temperature and power-law index of the temperature–density relations are shown in the bottom panel. The trends are the same as those shown in Fig. 2. We note that the overall effect depends only weakly on wavenumber for $k < 0.01$ s km^{-1} and steepens at smaller scales. Note that the dependence of the derivatives on k and z is distinctively different for the different parameters. This is the reason why we will be able to obtain reasonably tight constraints for most of them.

Our results agree quite well with the results of VHS and M04b. We note, however, that a direct quantitative comparison with M04b is not obvious. Our best-guess model has still somewhat different parameters from their fiducial model and M04b have used HPM simulations with a range of corrections while we have used full hydrodynamical simulations. One may ask how much these derivatives depend on our choice of the best-guess model. We have checked this for a few cases. The derivatives obtained by re-scaling the effective optical depth around other models (B1, B3 and C3) are different by less then 0.5 per cent compared to those shown in Fig. 3. The

derivatives with respect to σ_8 and n differ by less than 2.5 and 1.5 per cent, respectively, compared to expanding around B2. We have also directly compared the approximate flux power obtained with the Taylor expansion with that extracted from hydrodynamical simulations for a few simulations with parameters that are about $\gtrsim 2\sigma$ away from our best-guess model. For the $\sigma_8 = 0.7$ and $\sigma_8 = 1$ (60 400) the error of the approximation is less than 3.5 per cent which should be compared to the difference to the best-guess model which is ~ 10 per cent. We have also run a few further (30 200) simulations with $n = 1.05$, $\Omega_m = 0.34$ and a hotter simulation with $T_0 = 41\,000$ K and $\gamma = 1.56$. The approximations for the models with different Ω_m and the spectral index n are accurate to 1 per cent. The error for the model with the different T_0 parameter is ~ 5 per cent. By comparing with Fig. 3 we find that for $\gtrsim 2\sigma$ displacements in the parameters n, σ_8, ω_m and T_0 the error of the Taylor series approximation is generally less than 30 per cent of the difference between the models. This is not perfect but should be acceptable considering the expense of full-hydrodynamical simulations and the size of the parameter space.

5 CONSTRAINING ASTROPHYSICAL AND COSMOLOGICAL PARAMETERS

5.1 Summary of the free parameters of the χ^2 minimization

We have modified the code COSMOMC (Lewis & Bridle 2002) to run Monte Carlo–Markov Chains for our set of parameters. After settling on a best-guess model we have explored the parameter space close to the best-guess model. For most of the analysis we have used 22 parameters for the χ^2 minimization, some of them free while some of them independently constrained. We briefly summarize the parameters here.

We assume a flat cosmological model with a cosmological constant and neglect the possibility of a non-zero neutrino mass. There are thus four cosmological parameters that describe the matter distribution: the spectral index n, the DM power spectrum amplitude σ_8, Ω_m and H_0. We use nine 'astrophysical' parameters. Two describe the effective evolution of the optical-depth evolution, six describe the evolution of γ and T_0 and one describes the contribution of strong absorption systems. For the evolution of the optical depth we assume a power-law $\tau_{\mathrm{eff}}(z) = \tau_{\mathrm{eff}}^A(z{=}3)[(1{+}z)/4]^{\tau_{\mathrm{eff}}^S}$. Note that this is different from what we did when we fitted the suite of hydrodynamical simulations where we let the effective optical depth vary independently at all redshift bins. We will come back to this in Section 5.4.

For the evolution of γ and T_0 we assume broken power laws with a break at $z = 3$. The three parameters for the temperature are the amplitudes at $z = 3$, T_0^A ($z = 3$) and the two slopes $T_0^S(z < 3)$ and $T_0^S(z > 3)$. γ is described in the same way by γ^A ($z = 3$), $\gamma^S(z < 3)$ and $\gamma^S(z > 3)$. The correction for the damped/high-column density systems is modelled with the k dependence of fig. 11 of M04b and an overall amplitude A_{damp} and no redshift evolution, as described in Section 4.2.4

Finally, we have a total of nine parameters which model uncertainties in the correction to the data. Eight parameters for the noise correction f_i as described in Section 4.2.1 and one parameter α describing the error of the resolution correction. Note that all the parameters describing the errors of the corrections to the data and the correction for damped/high-column density systems are constrained as suggested in M04b and described in Section 4.2.

We will present here two sets of results. At first we will discuss the 1D and 2D likelihoods for the most significant parameters by
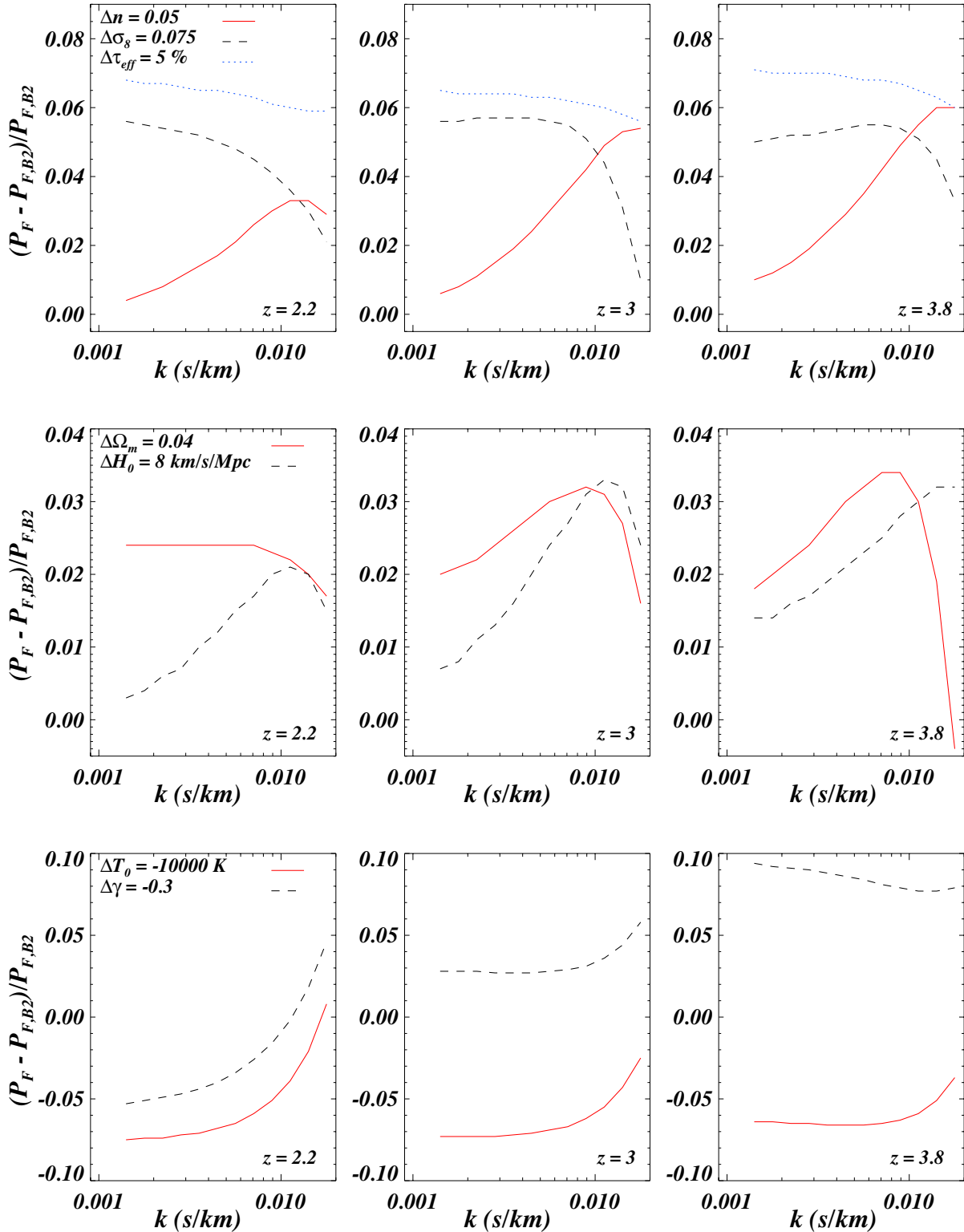
Figure 3. Top: fractional differences in the flux power spectrum for variations of σ_8 value (dashed curve), the spectral index n (continuous curve) and the effective optical depth $\tau_{\rm eff}$ (dotted curve) at $z = 2.2$, 3 and 3.8 (left-hand, centre and right-hand panel, respectively). Middle: fractional differences in the flux power spectrum for variations of $\Omega_{\rm m}$ value (continuous curve), the Hubble parameter H_0 (dashed curve). Bottom: fractional differences in the flux power spectrum for variations of γ (continuous curve) and T_0 (dashed curve).

assuming no priors on the cosmological and astrophysical parameters (with the exception of the correction for damped systems). Then we will show some results assuming priors on the Hubble parameter and on the thermal history.

5.2 Results without priors

The dashed curves in Fig. 4 show the 1D (marginalized) likelihoods for our full set of parameters without imposing any priors on the
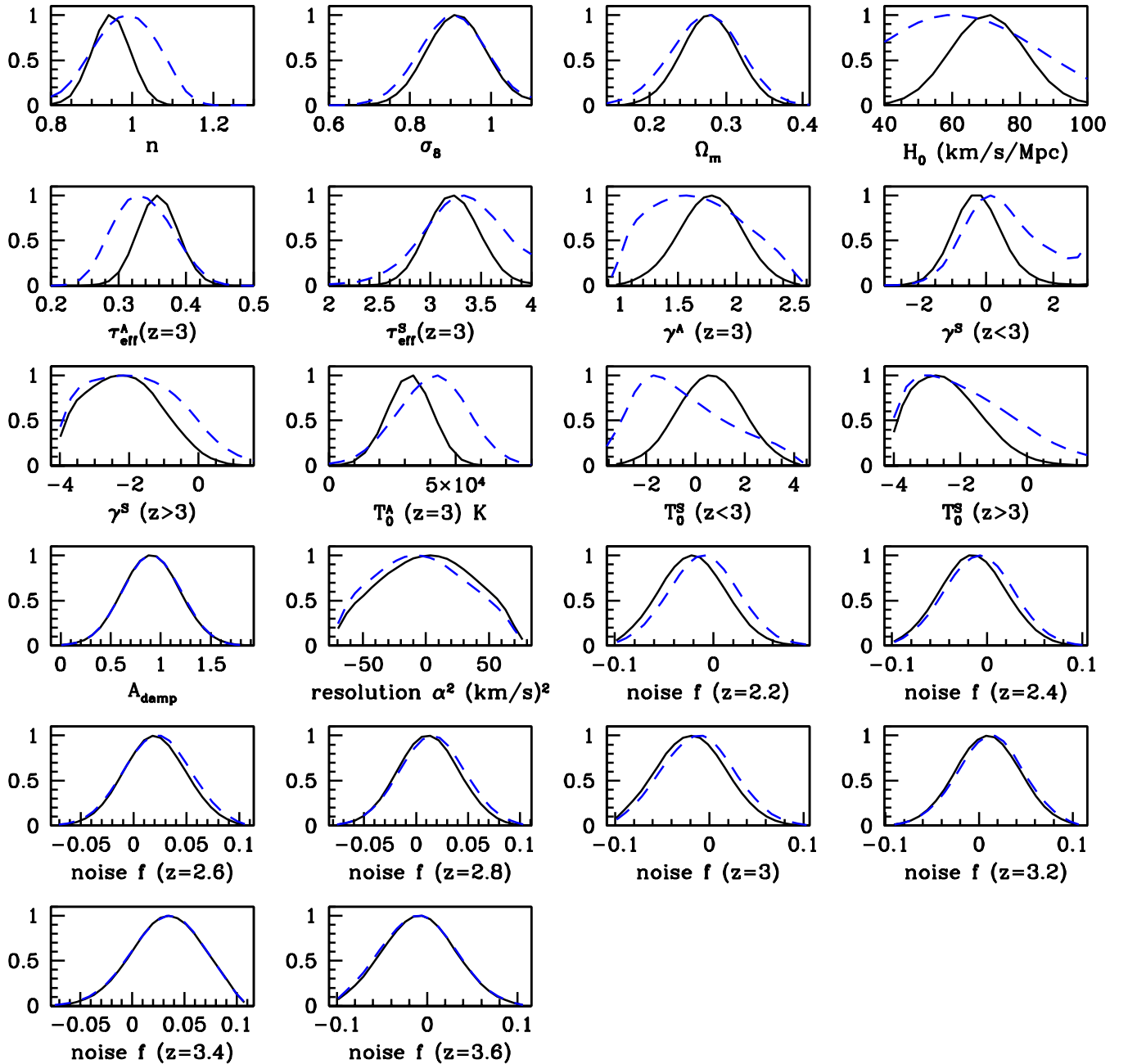
Figure 4. 1D marginalized likelihoods for our 22 parameters. Dashed curves represent the case without priors, while the continuous curves are obtained with the priors discussed in Section 5.3. Cosmological and astrophysical parameters were inferred with a Taylor expansion of the flux power spectrum of the best-guess model to first order.

cosmological and astrophysical parameters. The best-fitting model has now $\chi^2_{\min} = 78.9$ for 84 d.o.f. A χ^2 equal or larger than this should have a probability of 64 per cent. Our best-fitting model is thus an excellent fit, maybe with a hint that we are already marginally overfitting the data. Most parameters including σ_8, n and Ω_m are tightly constrained. The constraints on the thermal history are considerably weaker. This is not surprising as the rather low resolution of the SDSS spectra means that the thermal cut-off at small scales is not actually resolved. The best-fitting value for T_0^A is rather high, $(4.1 \pm 1.3) \times 10^4$ K, and may be in disagreement with the best-fitting values of M04b who find $T_0^A = 2 \times 10^4$ K without giving any error estimate.

The dashed curves in Fig. 5 show 2D likelihood contours for various parameter combinations. The contours have been obtained by marginalizing over the rest of the parameters. We note that the best-fitting models prefer somewhat larger values of the spectral index and higher temperatures than those of our best-guess model. The 2D contour plot of γ^A versus T_0^A, suggests that in order to reconcile this measurement with a colder IGM one would need an unplausibly steep temperature–density relation with $\gamma \sim 2$.

The preferred values for the thermal state of the IGM are actually outside the range suggested by a detailed analysis of the line width of the absorption feature using high-resolution spectra. This is shown in Fig. 6 where we compare the best-fitting evolution of
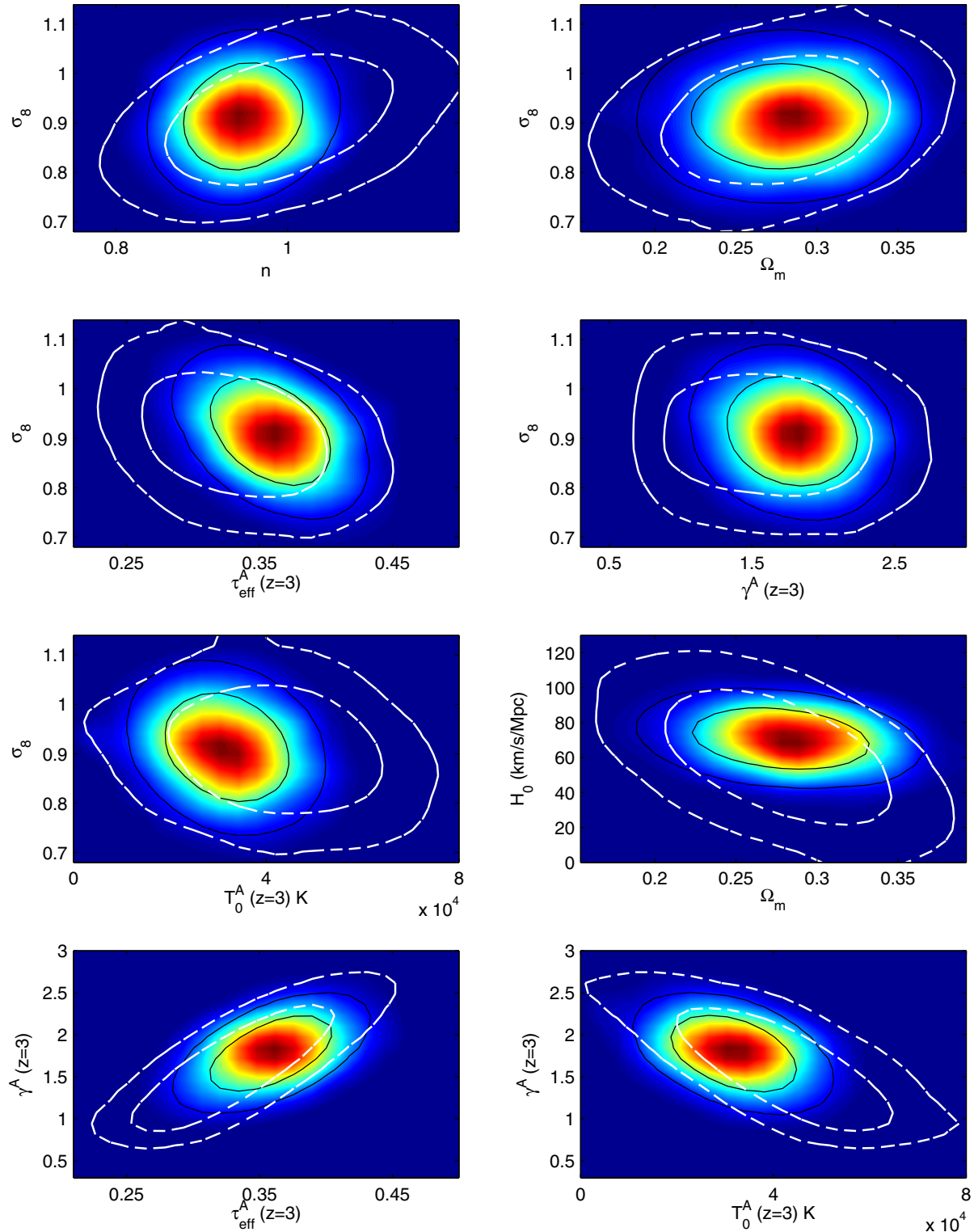
Figure 5. 2D likelihoods for some of the parameters used in our analysis. Filled (coloured), continuous and white dashed contours refer to the mean likelihood for the case with priors, the marginalized likelihood for the case with priors and the marginalized likelihood for the case without priors, respectively. Cosmological and astrophysical parameters were inferred with a Taylor expansion of the flux power spectrum of the best-guess model to first order.

the temperature T_0 (hashed region) to the measurements of the temperature by Schaye et al. (2000). Note again that the lower range of values corresponds to $\gamma \gtrsim 2$ outside of the range of plausible values for a photoionized IGM. The Hubble constant is also only

poorly constrained. This is again not surprising as the spectra are sensitive to the matter power spectrum in velocity space. The only dependence comes thus through the shape parameter $\Gamma = \Omega_m\, h$, which is weak (Fig. 3).
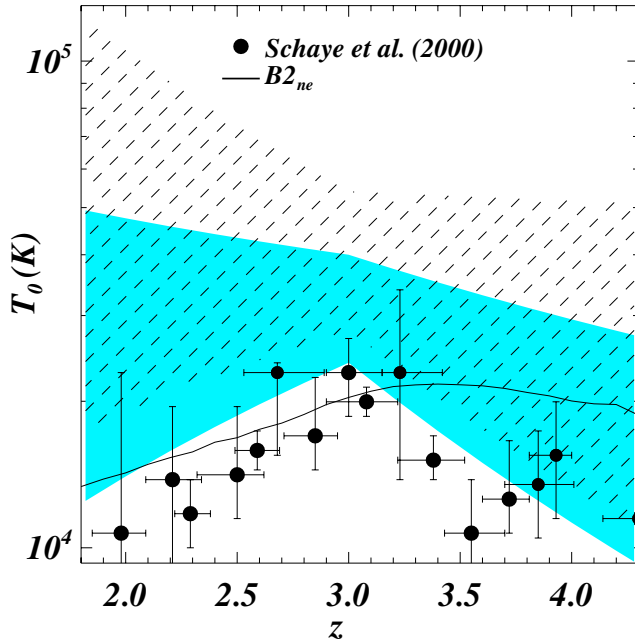
Figure 6. Evolution of the temperature at the mean density T_0 with redshift inferred for our analysis without priors (hashed area) and with priors (shaded area). The regions indicate 1σ uncertainties. The observational points by Schaye et al. (2000) and the thermal evolution of our simulation of model B2 with the non-equilibrium solver are also shown.

Table 2. Cosmological and astrophysical parameters inferred with a Taylor expansion of the flux power spectrum of the best-guess model to first order (1σ error bars).

Parameter	Without priors	With priors on thermal history and H_0
n	0.98 ± 0.07	0.95 ± 0.04
σ_8	0.90 ± 0.08	0.91 ± 0.07
Ω_m	0.27 ± 0.04	0.28 ± 0.03
H_0 (km s^{-1} Mpc^{-1})	62 ± 20	70 ± 10
τ_{eff}^A ($z = 3$)	0.337 ± 0.040	0.359 ± 0.027
τ_{eff}^S	3.29 ± 0.36	3.22 ± 0.24
γ^A ($z = 3$)	1.67 ± 0.38	1.78 ± 0.26
γ^S ($z < 3$)	0.71 ± 1.26	-0.21 ± 0.74
γ^S ($z > 3$)	-1.83 ± 1.03	-2.15 ± 1.00
T_0 ($z = 3$) (10^4) K	4.1 ± 1.3	3.2 ± 0.8
T_0^S ($z < 3$)	-0.49 ± 1.83	0.60 ± 1.27
T_0^S ($z > 3$)	-1.78 ± 1.58	-2.38 ± 1.01
A_{damp}	0.91 ± 0.28	0.91 ± 0.27

The best-fitting values for our modelling without priors with errors obtained by marginalizing over all other parameters are listed in Table 2.

As a further consistency check and to test how well the observed redshift evolution of the flux power spectrum probes the expected gravitational growth of structure we have also obtained constraints on σ_8 and n independently for each redshift bin. We get the following constraints for σ_8: 0.92 ± 0.16, 0.89 ± 0.11, 0.98 ± 0.13, 1.02 ± 0.95, 0.94 ± 0.78, 0.88 ± 0.09, 0.87 ± 0.12, 0.95 ± 0.16 and 0.90 ± 0.17 for $z = 2.2$, 2.4, 2.6, 2.8, 3, 3.2, 3.4, 3.6 and 3.8, respectively. For n we get: 0.88 ± 0.09, 0.97 ± 0.07, 0.89 ± 0.08, 0.90 ± 0.06, 0.90 ± 0.06, 0.94 ± 0.07, 0.99 ± 0.06, 0.90 ± 0.05 and 0.95 ± 0.14 for $z = 2.2$, 2.4, 2.6, 2.8, 3, 3.2, 3.4, 3.6 and 3.8, respectively.

The total $\chi^2_{\min}$ is 77.9 for 74 d.o.f. in this case. The constraints are weaker but perfectly consistent with our estimates from all redshift bins combined. The errors are significantly smaller than the expected growth of the amplitude between the lower and upper redshift end of the sample demonstrating that the flux power spectrum evolves as expected for gravitational growth.

5.3 Results with priors

As discussed in the last section the SDSS flux power spectrum published by M04a prefers unplausibly large temperatures for reasonable values of γ. We have thus repeated the analysis with (Gaussian) priors on the thermal state of the IGM, as follows: $T_0^A(z = 3) = (2.1 \pm 0.7) \times 10^4$, $T_0^S(z < 3) = 1.45 \pm 1.00$ and $T_0^S(z > 3) = -2.44 \pm 1.00$ (Schaye et al. 2000). We have also added a prior on the Hubble constant, $H_0 = 72 \pm 8$ km s^{-1} Mpc^{-1} (Freedman et al. 2001).

The solid curves in Figs 4 and 5 show the marginalized likelihoods for our analysis with priors. The filled (coloured) contours in Fig. 5 show the mean 2D likelihood. As expected the thermal parameters and the Hubble constant are now more tightly constrained. The temperature evolution of the best-fitting model with prior is shown as the shaded region in Fig. 6. It lies about 1σ above the imposed constraint suggesting that the observed flux power spectrum definitely prefers models with higher temperatures than those observed. Rather than being an actual indication of higher temperature this is more likely indicative of a non-understood systematic uncertainty in our modelling which makes the flux power spectrum mimic high temperatures. As discussed in Section 4.2.5 there are plenty of candidates for this.

The best-fitting model with priors has $\chi^2_{\min} = 83.1$ for 88 d.o.f. A χ^2 equal or larger than this should have a probability of 60 per cent very similar to the case without priors. The best-fitting values for our modelling without priors are also listed in Table 2 (right-hand column).

The most significant change caused by the introduction of the priors is a decrease of the spectral index by $\Delta n = 0.03$ (consistent with the 1σ errors). In Fig. 5, the strongest correlations are those in the $\sigma_8 - \tau_{\mathrm{eff}}^A$, $\gamma^A - T_0^A$ and $\gamma^A - \tau_{\mathrm{eff}}$ planes. As expected a higher value of the τ_{eff}^A requires a smaller σ_8 quantitatively comparable to previous findings (Viel et al. 2004c; VHS; Seljak et al. 2003). The best-fitting temperature and slope of temperature–density relation are again anti-correlated. A lower temperature corresponds to a steeper temperature–density relation. We further note that σ_8 and n appear not to be correlated, in contrast to the corresponding parameters (Δ_L^2, n_{eff}) in M04b. If we take out the box-size and resolution corrections we do not get significant changes in the final parameters but the $\chi^2_{\min}$ increases by 1.3, showing that the data prefer these corrections. The best-fitting values for our modelling with priors with errors obtained by marginalizing over all other parameters are also listed in Table 2.

5.4 The inferred evolution of the effective optical depth

As discussed before the effective optical depth is the largest uncertainty and it is very degenerate with the fluctuation amplitude. Larger effective optical depths correspond to smaller σ_8 values (Fig. 5). The shape of the derivative of the flux power spectrum with respect to τ_{eff} and σ_8 (Fig. 3) is, however, sufficiently different to get still interesting constraints on τ_{eff}.

In the left-hand panel of Fig. 7 we compare the best-fitting τ_{eff} for our set of (60 400) hydrodynamical simulations to measurements made from high- and low-resolution spectra. All values are shown
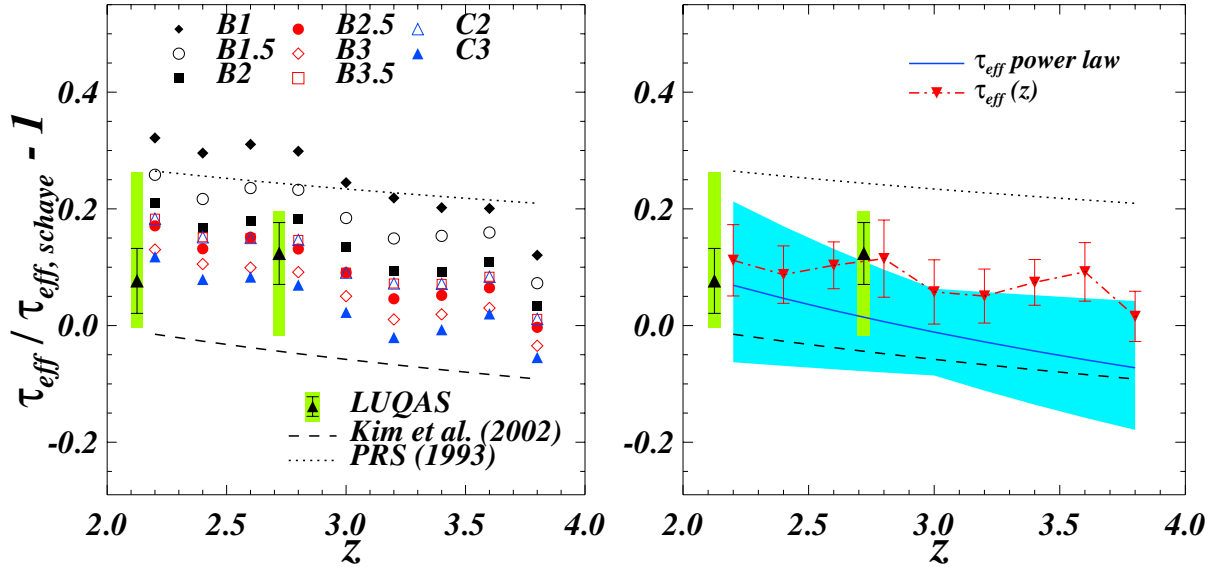
Figure 7. Left-hand panel: fractional differences of the best-fitting value of the effective optical depth with respect to the evolution found by Schaye et al. (2003) for some of the models of Table 1 (with the effective optical depth in the eight redshift bins as the only free parameters). The observed values obtained for the LUQAS sample are represented by triangles, while the shaded bars indicate the range used in the analysis by VHS. The dotted line and the dashed line show the observed evolution found by Kim et al. (2002) and Press et al. (1993), respectively. Right-hand panel: same as in the left-hand panel but using the flux power spectra calculated using a Taylor expansion to first order around the 'best-guess' model B2. For the continuous curve the effective optical depth was assumed to evolve as a power law with redshift while the triangles show the case of leaving the optical depth float freely in all redshift bins.

relative to the fit to the observed evolution of the optical depth corrected for the contribution by associated metal absorption based on a set of high-resolution spectra by Schaye et al. (2003) (their fig. 1). The fit is given by $\tau_{\rm eff} = 0.363\,[(1+z)/4]^{3.57}$. The evolution obtained by Kim et al. (2002) based on a different set of high-resolution spectra is shown as the dashed curve. The measurements at $z = 2.125$ and 2.72 made by VHS from the LUQAS sample (Kim et al. 2004) are shown as filled triangles. Note that there is some overlap between the Schaye et al. (2003) data set and the LUQAS sample of K04. The dotted line shows the result of Press, Rybicki & Schneider (PRS, 1993) from low-resolution spectra of rather poor quality. The shaded area shows the range adopted by VHS and Viel et al. (2004c) for their analysis. The different symbols show the results from our fits of the flux power spectrum of the hydrodynamical simulations to the SDSS flux power spectrum as described in Section 4.3. The degeneracy between σ_8 and $\tau_{\rm eff}$ is clearly visible and can be roughly described by $\Delta\tau_{\rm eff}/\tau_{\rm eff} = 0.8\,\Delta\sigma_8$ similar to that found in VHS.

In the right-hand panel, the solid curve shows the evolution of $\tau_{\rm eff}$ for our best-fitting model compared to the same observational estimates. As discussed we have modelled the evolution of $\tau_{\rm eff}$ as a power law. We find $\tau_{\rm eff}(z) = (0.359 \pm 0.027)\,[(1+z)/4]^{3.22\pm0.24}$ in agreement with Schaye et al. (2003) and the values used by VHS. It also agrees well with the values inferred by Lidz et al. (2005) from the flux probability distribution. The shaded area in the right-hand panel shows the 1σ uncertainty of the best-fitting model. We thus confirm the findings of M04b that the differences in the k dependence of the respective changes can break the degeneracy between σ_8 and $\tau_{\rm eff}$. The dot–dashed line and the triangles show the evolution of the optical depth if we let $\tau_{\rm eff}$ vary separately at all nine redshifts (this increases the number of free parameters from 22 to 28). Letting the effective optical depth vary freely at high redshift increases the average inferred effective optical depth by about 5 per cent and reduces the inferred errors.

Table 3. Cosmological parameters obtained in recent studies of the Lyα forest.

	σ_8	n
Spergel et al. (2003)[a]	0.9 ± 0.1	0.99 ± 0.04
Spergel et al. (2003)[b]	–	0.96 ± 0.02
Viel et al. (2004b)[c]	0.93 ± 0.10	1.01 ± 0.06
Viel et al. (2004c)[d]	0.94 ± 0.08	0.99 ± 0.03
Desjacques et al. (2004)	0.90 ± 0.05	–
Tytler et al. (2004)	0.90	–
McDonald et al. (2004b)[e]	0.85 ± 0.06	0.94 ± 0.05
Seljak et al. (2005)[f]	0.89 ± 0.03	0.99 ± 0.03
This work (priors case)	0.91 ± 0.07	0.95 ± 0.04

[a]*WMAP* only. [b]*WMAP* ext + 2dF + Lyα (no running of the spectral index). [c]LUQAS + Croft et al. (2002) only. [d]LUQAS + Croft et al. (2002) + *WMAP* 1st year. [e]Error bars extrapolated by the authors from the abstract of M04b. [f]SDSS Lyα flux power spectrum + *WMAP*.

6 DISCUSSION AND CONCLUSION

6.1 Comparison with previous results for σ_8 and n

In Table 3, we list results for the most important parameters describing the matter distribution (σ_8 and n) obtained by recent studies using the Lyα forest by a variety of authors. The most direct comparison is again with M04b. At $z = 3$ our results correspond to a fluctuation amplitude and effective slope at the pivot wavenumber $k = 0.009\,{\rm s\,km}^{-1}$ as defined by M04b of $\Delta_{\rm L}^2 = 0.40 \pm 0.06$ and $n_{\rm eff} = -2.33 \pm 0.05$. The values are consistent within 1σ with those of M04b. The agreement with other authors including our own work is at the same level. For comparison we also show the value for *WMAP* alone. A consistent picture emerges for the Lyα forest data with a rather high-fluctuation amplitude and no evidence for a significant

deviation from $n = 1$ or a running of the spectral index. These results hold for the Lyα forest data alone but are considerably strengthened if the Lyα forest data are combined with the CMB and other data.

6.2 Remaining uncertainties and future progress

As discussed in Section 4.2 there are many systematic uncertainties that affect the measurement of cosmological parameters with the Lyα flux power spectrum.

In order to test the stability of the results we have removed the correction for high-column density systems and the errors for the noise and resolution corrections in the case with priors. If we take out the correction due to strong-absorption systems, n decreases to 0.93 ± 0.04, and the best-fitting value for $\tau_{\rm eff}$ ($z = 3$) becomes 0.381, all the other parameters remain practically unchanged. The measured values do therefore practically not change but the value of $\chi^2_{\rm min}$ increases by 0.5. If we do not allow for the error to the noise and resolution corrections the inferred values do again not change but the value of $\chi^2_{\rm min}$ increases by 1.8. Note that M04a have also subtracted an estimate of the contribution of associated metal absorption from the flux power spectrum and have applied a suite of other (smaller) corrections to the data (see M04a for more details). Many of these corrections would either not be necessary or substantially easier for spectra with somewhat better resolution ($R \sim 10000$) and higher S/N. Obtaining large samples of such spectra is observationally feasible and there is certainly room for improvement. Note further that the SDSS team will soon release a further measurement of the flux power spectrum performed by an independent group within the collaboration.

We also note again that calculating the flux power spectrum by using a Taylor expansion to first order around the best-guess model is just an approximation. This was an important part of our analysis as it reduced the amount of CPU time necessary dramatically, but could be further improved by getting more accurate fits around the 'best-guess' model. We have also not attempted to correct for the possible effects of spatial fluctuations of the H I ionization rate, galactic winds, temperature fluctuation or the re-ionization history. This is because we are not convinced that it is already possible to model these effects with sufficient accuracy. This should hopefully change in future with improved observational constraints and numerical capabilities. One should further keep in mind that so far very little cross-checking of hydrodynamical simulation run with different codes has been performed.

In our study the rather poorly known thermal state of the IGM is one of the major remaining uncertainties. Further high-resolution spectroscopy and improved modelling will hopefully soon improve this. Accurate modelling of the effect of high-column density systems/damped Lyα systems and improvement in the determination of the column density distribution of observed absorption systems in the poorly determined range around $\log N \sim 17$ should also be a priority in further studies [see the discussion in McDonald et al. 2005].

It is certainly encouraging that the differences between our analysis and that of M04b are moderate despite considerable differences between their approximate HPM simulations calibrated with hydrodynamical simulations of rather small box size and our analysis with full hydrodynamical simulations of much larger box size here and in VHS.

For the time being we would advise the conservative reader to double the formal errors quoted here. This will bring the error estimates to about the same size as the conservative estimates for the errors of the fluctuation amplitude from the Lyα forest data alone in the analysis of VHS. The actual errors lie probably somewhere in between.

6.3 Conclusions

We have compared the flux power spectra calculated from a suite of full large box-size high-resolution ($60\,h^{-1}$ Mpc, 2×400^3 particles) hydrodynamical simulations with the SDSS flux power spectrum as published by McDonald et al. (2005). We have identified a best-guess model which provides a good fit to the data. We have used a Taylor expansion to first order to calculate flux power spectra in a multidimensional space of parameters describing the matter power spectrum and the thermal history of the IGM with values close to those of our best-guess model. We have investigated the combined effect of cosmological and astrophysical parameters on the flux power spectrum with an adapted version of the Markov Chain code COSMOMC. Our main results can be summarized as follows.

(i) The flux power spectrum calculated directly from the simulation of a LambdaCDM (ΛCDM) model ($\Omega_{\rm m} = 0.26$, $\Omega_{\Lambda} = 0.74$, $\Omega_{\rm b} = 0.0463$ and $H_0 = 72\,{\rm km\,s^{-1}\,Mpc^{-1}}$, $\sigma_8 = 0.925$) with a temperature–density relation described by $T_0(z = 3) = 21\,000$ and $\gamma(z = 3) = 1.6$ gives an acceptable fit to the SDSS flux power spectrum in the redshift range $2.2 < z < 3.6$ ($\chi^2 \sim 101$ for 88 d.o.f.). The fit can easily be further improved by small changes in the cosmological and astrophysical parameters.

(ii) At higher redshift the deviations from the observed flux power spectrum become significantly larger ($\Delta\chi^2 = 26$ for 12 additional data points at $z = 3.8$) suggesting either some problem with the data or a physical effect that changes rapidly with redshift.

(iii) We confirm the claim by McDonald et al. (2004) that the degeneracy of the dependence of the flux power spectrum on the amplitude of the matter power spectrum and the effective optical depth can be broken for the published SDSS flux power spectrum. It will be interesting to see if the same is true for the independent analysis of the SDSS data to be released soon.

(iv) The SDSS power spectrum alone can constrain the amplitude of the matter power spectrum, the matter density and the power-law index of primordial density fluctuation to within $\sim$ 5–10 per cent. The thermal state of the IGM is, however, poorly constrained and the SDSS power spectrum formally prefers models with unplausible values of the parameters describing the thermal state. The dependence of the flux power spectrum on the assumed Hubble constant is also very weak and the Hubble constant is not well constrained. The exact values for the other cosmological parameters depend somewhat on the assumed prior for the thermal state and the details of the correction which have been applied to the data.

(v) With a prior on the thermal history and the Hubble constant motivated by the observations by Schaye et al. (2000) and Freedman et al. (2001) we obtain the following best-fitting values for the cosmological parameters $\Omega_{\rm m} = 0.28 \pm 0.03$, $n = 0.95 \pm 0.04$ and $\sigma_8 = 0.91 \pm 0.07$ (1σ error bars), and the effective optical depth is well described by the following power-law relation: $\tau_{\rm eff}(z) = (0.359 \pm 0.027)\,[(1 + z)/4]^{3.22 \pm 0.24}$. The errors were obtained by marginalizing over a set of 22 parameters describing the matter distribution, thermal history of the Universe, the effective optical depth and errors to various corrections to the data. The values for σ_8 and n are consistent with those found by M04a for the same data set with different simulations. They are also consistent with the results of other recent studies of Lyα forest data. The inferred optical depth is in

good agreement with that measured directly from continuum-fitted high-quality absorption spectra.

REFERENCES

Abel T., Haehnelt M. G., 1999, ApJ, 520, 13
Adelberger K. L., Shapley A. E., Steidel C. C., Pettini M., Erb D. K., Reddy N. A., 2005, ApJ, 629, 636
Beltran M., Garcia-Bellido J., Lesgourgues J., Viel M., 2005, Phys. Rev. D, in press
Bolton J. S., Haehnelt M. G., Viel M., Springel V., 2005a, MNRAS, 357, 1178
Bolton J. S., Haehnelt M. G., Viel M., Carswell R. F., 2005b, MNRAS, submitted (astro-ph/0508201)
Cowie L., Songaila A., Kim T.-S., Hu E. M., 1995, AJ, 109, 1522
Croft R. A. C., 2004, ApJ, 610, 642
Croft R. A. C., Weinberg D. H., Katz N., Hernquist L., 1998, ApJ, 495, 44
Croft R. A. C., Weinberg D. H., Bolte M., Burles S., Hernquist L., Katz N., Kirkman D., Tytler D., 2002, ApJ, 581, 20 (C02)
Desjacques V., Nusser A., 2005, MNRAS, 361, 1257
Desjacques V., Nusser A., Haehnelt M. G., Stoehr F., 2004, MNRAS, 350, 879
Eisenstein D. J., Hu W., 1999, ApJ, 511, 5
Freedman W. L. et al., 2001, ApJ, 553, 47
Gnedin N. Y., Hamilton A. J. S., 2002, MNRAS, 334, 107
Gnedin N. Y., Hui L., 1998, MNRAS, 296, 44
Haardt F., Madau P., 1996, ApJ, 461, 20
Hui L., Gnedin N., 1997, MNRAS, 292, 27
Hui L., Burles S., Seljak U., Rutledge R. E., Magnier E., Tytler D., 2001, ApJ, 552, 15
Lewis A., Bridle S., 2002, Phys. Rev. D, 66, 103511; http://www.cosmologist.info
Lidz A., Heitmann K., Hui L., Habib S., Rauch M., Sargent W. L. W., 2005, preprint (astro-ph/0505138)
Kim T.-S., Carswell R. F., Cristiani S., D'Odorico S., Giallongo E., 2002, MNRAS, 335, 555
Kim T.-S., Viel M., Haehnelt M. G., Carswell R. F., Cristiani S., 2004, MNRAS, 347, 355 [K04]

Kollmeier J., Miralda-Escude J., Cen R., Ostriker J. P., 2005, ApJ, submitted (astro-ph/0503674)
Kollmeier J. A., Weinberg D. H., Davé R., Katz N., 2003, ApJ, 594, 75
McDonald P., 2003, ApJ, 585, 34
McDonald P., Miralda-Escudé J., Rauch M., Sargent W. L., Barlow T. A., Cen R., Ostriker J. P., 2000, ApJ, 543, 1
McDonald P. et al., 2004a, preprint (astro-ph/0407377) (M04a)
McDonald P. et al., 2004b, preprint (astro-ph/0407378) (M04b)
McDonald P., Seljak U., Cen R., Bode P., Ostriker J. P., 2005, MNRAS, 360, 1471
Meiksin A., White M., 2004, MNRAS, 350, 1107
Pieri M., Haehnelt M. G., 2004, MNRAS, 347, 985
Press W. H., Rybicki G. B., Schneider D. P., 1993, ApJ, 414, 64
Rauch M., Becker G. D., Viel M., Sargent W. L. W., Smette A., Simcoe R. A., Barlow T. A., Haehnelt M., 2005, ApJ, 632, 58
Ricotti M., Gnedin N., Shull M., 2000, ApJ, 534, 41
Schaye J., Aguirre A., Kim T.-S., Theuns T., Rauch M., Sargent W. L. W., 2003, ApJ, 596, 768
Schaye J., Theuns T., Rauch M., Efstathiou G., Sargent W. L. W., 2000, MNRAS, 318, 817
Seljak U., McDonald P., Makarov A., 2003, MNRAS, 342, L79
Seljak et al., 2005, Phys. Rev. D, 71, 103515
Springel V., 2005, MNRAS, in press (doi:10.1111/j.1365-2966. 2005.09655.x) (astro-ph/0505010)
Springel V., Hernquist L., 2002, MNRAS, 333, 649
Springel V., Yoshida N., White S. D. M., 2001, New Astron., 6, 79
Spergel D. N. et al., 2003, ApJS, 148, 175
Theuns T., Leonard A., Efstathiou G., Pearce F. R., Thomas P. A., 1998, MNRAS, 301, 478
Theuns T., Schaye J., Haehnelt M. G., 2000, 315, 600
Theuns T., Viel M., Kay S., Schaye J., Carswell B., Tzanavaris P., 2002a, ApJ, 578, L5
Theuns T., Zaroubi S., Kim T.-S., Tzanavaris P., Carswell R. F., 2002b, MNRAS, 332, 367
Tytler et al., 2004, ApJ, 617, 1
Verde L. et al., 2003, ApJS, 148, 195
Viel M., Matarrese S., Theuns T., Munshi D., Wang Y., 2003, MNRAS, 340, L47
Viel M., Haehnelt M. G., Carswell R. F., Kim T.-S., 2004a, MNRAS, 349, L33
Viel M., Haehnelt M. G., Springel, 2004b, MNRAS, 354, 684 (VHS)
Viel M., Weller J., Haehnelt M. G., 2004c, MNRAS, 355, L23
Viel M., Lesgourgues J., Haehnelt M. G., Matarrese S., Riotto A., 2005a, Phys. Rev. D, 71, 063534
Viel M., Haehnelt M. G., Springel, 2005b, MNRAS, submitted (astro-ph/0504641)
Zaldarriaga M., Hui L., Tegmark M., 2001, ApJ, 557, 519
Zaldarriaga M., Scoccimarro R., Hui L., 2003, ApJ, 590, 1

This paper has been typeset from a TeX/LaTeX file prepared by the author.